nature chemistry

ARTICLES

PUBLISHED ONLINE: 19 OCTOBER 2015 | DOI: 10.1038/NCHEM.2370

A labile hydride strategy for the synthesis of heavily nitridized $BaTiO_3$

Takeshi Yajima[1,2], Fumitaka Takeiri[1], Kohei Aidzu[1], Hirofumi Akamatsu[3], Koji Fujita[4], Wataru Yoshimune[1], Masatoshi Ohkura[1], Shiming Lei[3], Venkatraman Gopalan[3], Katsuhisa Tanaka[4], Craig M. Brown[5], Mark A. Green[6], Takafumi Yamamoto[1], Yoji Kobayashi[1] and Hiroshi Kageyama[1,7]*

Oxynitrides have been explored extensively in the past decade because of their interesting properties, such as visible-light absorption, photocatalytic activity and high dielectric permittivity. Their synthesis typically requires high-temperature NH_3 treatment (800–1,300 °C) of precursors, such as oxides, but the highly reducing conditions and the low mobility of N^{3-} species in the lattice place significant constraints on the composition and structure—and hence the properties—of the resulting oxynitrides. Here we show a topochemical route that enables the preparation of an oxynitride at low temperatures (<500 °C), using a perovskite oxyhydride as a host. The lability of H^- in $BaTiO_{3-x}H_x$ ($x \leq 0.6$) allows H^-/N^{3-} exchange to occur, and yields a room-temperature ferroelectric $BaTiO_{3-x}N_{2x/3}$. This anion exchange is accompanied by a metal-to-insulator crossover via mixed O–H–N intermediates. These findings suggest that this 'labile hydride' strategy can be used to explore various oxynitrides, and perhaps other mixed anionic compounds.

Mixed anion compounds, such as oxychlorides, oxychalcogenides, oxyhydrides and oxynitrides, are an emerging class of materials with intriguing properties unattainable in oxides. For instance, the incorporation of nitrogen into the oxide lattice results in a narrowing of the bandgap of d^0 oxides by shifting the valence-band edge upwards, because nitrogen is less electronegative than oxygen. This region is responsible for the absorption of visible light and makes it possible to use these materials as visible-light photocatalysts ($TiO_{2-x}N_x$, $Ga_{1-x}Zn_xN_{1-x}O_x$)[1,2] for water splitting, the decomposition of organic compounds and as non-toxic inorganic pigments ($Ca_{1-x}La_xTaO_{2-x}N_{1+x}$)[3]. Additionally, d^0 oxynitrides offer promising potential in dielectrics and other electronic properties. The lower electronegativity, higher electronic polarizability and higher formal charge of nitride relative to oxide can stabilize cation displacements through a second-order Jahn–Teller distortion, which leads to remarkably high dielectric constants in $BaTaO_2N$ (refs 4–6) and substrate-assisted (partial) ferroelectricity in $SrTaO_2N$ (ref. 7). $EuNbO_2N$ exhibits colossal magnetoresistivity, with $Eu^{2+}(4f^7)$–$Nb^{5+}(4d^0)$ interactions enhanced by covalent bonding to N (ref. 8).

The synthesis of oxynitrides is normally carried out by high-temperature ammonolysis, in which suitable precursors, typically oxides and carbonates, are reacted with a stream of ammonia at elevated temperatures (800–1,300 °C)[9,10]. The reaction mechanism of thermal ammonolysis is not fully understood yet, but it is suggested that NH_3 dissociates at the surface to form active nitriding species (N, NH, NH_2) and H_2 gas. The H_2 gas reacts with the lattice oxygen to form water and nitrogen is introduced into the lattice. A high temperature is required to allow diffusion of both the cations and the anions. The difficulty in the migration of N^{3-}, with its high charge, at moderate temperatures restricts the nitridization such that it occurs only at the surface. Although several alternative methods, such as ammonothermal synthesis and a urea-based route, are reported, these methods only yield known oxynitrides[11,12].

Among oxynitrides, the most studied are perovskite-type compounds that contain d^0 transition-metal ions (M, for example, Ti^{4+}, Zr^{4+}, Nb^{5+} and Ta^{5+}), which is largely because of the tolerance of these cations against reduction during high-temperature ammonolysis (that is, highly reducing). A large number of perovskite oxynitrides with the formulae AMO_2N, $AMON_2$, $AMO_{3-x}N_x$ and $AMO_{2-x}N_{1+x}$ (where A is an alkaline-earth or rare-earth element, $0 \leq x \leq 1$) have been reported[9,10,13,14]. However, once A and M are chosen, the anion composition is automatically set such that total charge neutrality is satisfied, for example $(La^{3+})(Ti^{4+})(O^{2-})_2(N^{3-})$, $(Sr^{2+})(Nb^{5+})(O^{2-})_2(N^{3-})$ and $(Ca^{2+})_{1-x}(La^{3+})_x(Ta^{5+})(O^{2-})_{2-x}(N^{3-})_{1+x}$. Although anion vacancies may be present, in reality the amount appears to be small and difficult to control. Such a constraint severely limits compositional and structural variations of oxynitrides and thus calls for alternative approaches for the synthesis.

In coordination chemistry, a complex in which ligands can undergo a rapid exchange reaction is classified as a labile complex[15]. In this study, we attempt to extend this concept in coordination chemistry to topochemical reactions of extended solids to access a new type of oxynitride using a recently reported perovskite oxyhydride, $BaTiO_{3-x}H_x$ ($0 \leq x \leq 0.6$)[16]. As the hydride ion (H^-) possesses a smaller mass and charge (relative to O^{2-}) and is prone to reacting with oxidizers or acids, the H^- in the TiO_5H or TiO_4H_2 octahedron is quite reactive and thus can be considered to act in a similar manner to a labile ligand. The labile nature of the H^- ligand is, indeed, seen in the hydride exchangeability of $BaTiO_{3-x}H_x$ at low temperatures; under a D_2 flow at 400 °C,

[1]Department of Energy and Hydrocarbon Chemistry, Graduate School of Engineering, Kyoto University, Nishikyo-ku, Kyoto 615-8510, Japan. [2]Institute for Solid State Physics, The University of Tokyo, Kashiwa, Chiba 277-8581, Japan. [3]Department of Materials Science and Engineering, Pennsylvania State University, University Park, Pennsylvania 16802, USA. [4]Department of Material Chemistry, Graduate School of Engineering, Kyoto University, Katsura, Nishikyo-ku, Kyoto 615-8510, Japan. [5]NIST Center for Neutron Research, National Institute of Standards and Technology, 100 Bureau Drive, MS 6100, Gaithersburg, Maryland 20899-6100, USA. [6]School of Physical Sciences, University of Kent, Canterbury, Kent CT2 7NH, UK. [7]CREST, Japan Science and Technology Agency, 7-3-1 Hongo, Bunkyo-ku, Tokyo 113-0033, Japan. *e-mail: kage@scl.kyoto-u.ac.jp

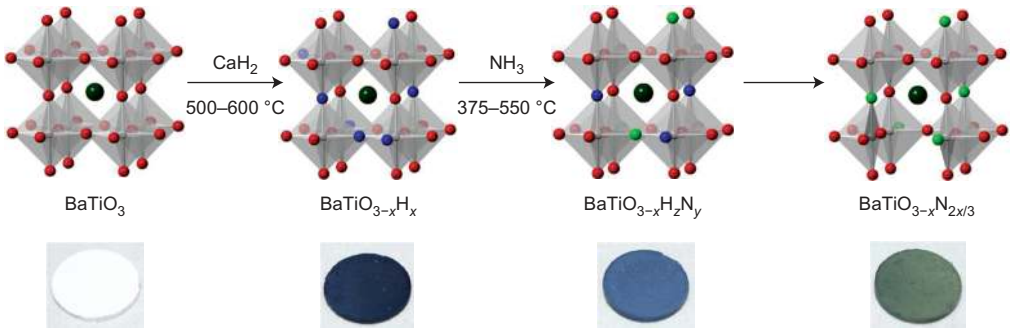

Figure 1 | Two-step synthesis of oxynitride $BaTiO_{3-x}N_{2x/3}$. Perovskite $BaTiO_3$ (oxide) converted to $BaTiO_{3-x}H_x$ (oxyhydride) by CaH_2 reduction[16]. $BaTiO_{3-x}H_x$ is converted into $BaTiO_{3-x}N_{2x/3}$ (oxynitride) by the low-temperature NH_3 treatment (this work), via the oxyhydride–nitride $BaTiO_{3-x}H_zN_y$. Ba, dark green; Ti, light grey; O, red; H, blue; N, light green. Here the lability of H^- in the oxyhydride allows H^-/N^{3-} exchange to occur by low-temperature ammonolysis (375–550 °C) to yield $BaTiO_{3-x}N_{2x/3}$ via mixed O-H-N intermediates. The photos displayed below each structure show the colour change of the specimens for $x = 0.6$. Compositions are approximated (left to right) as $BaTiO_3$ (Ti^{4+}), $BaTi^{3.4+}O_{2.4}H_{0.6}$ ($Ti^{3.4+}$), $BaTiO_{2.4}H_{0.14}N_{0.22}$ ($Ti^{3.6+}$) and $BaTiO_{2.4}N_{0.4}$ (Ti^{4+}). The colour change is related to the amount of Ti 3*d* t_{2g} electrons (see the text for details).

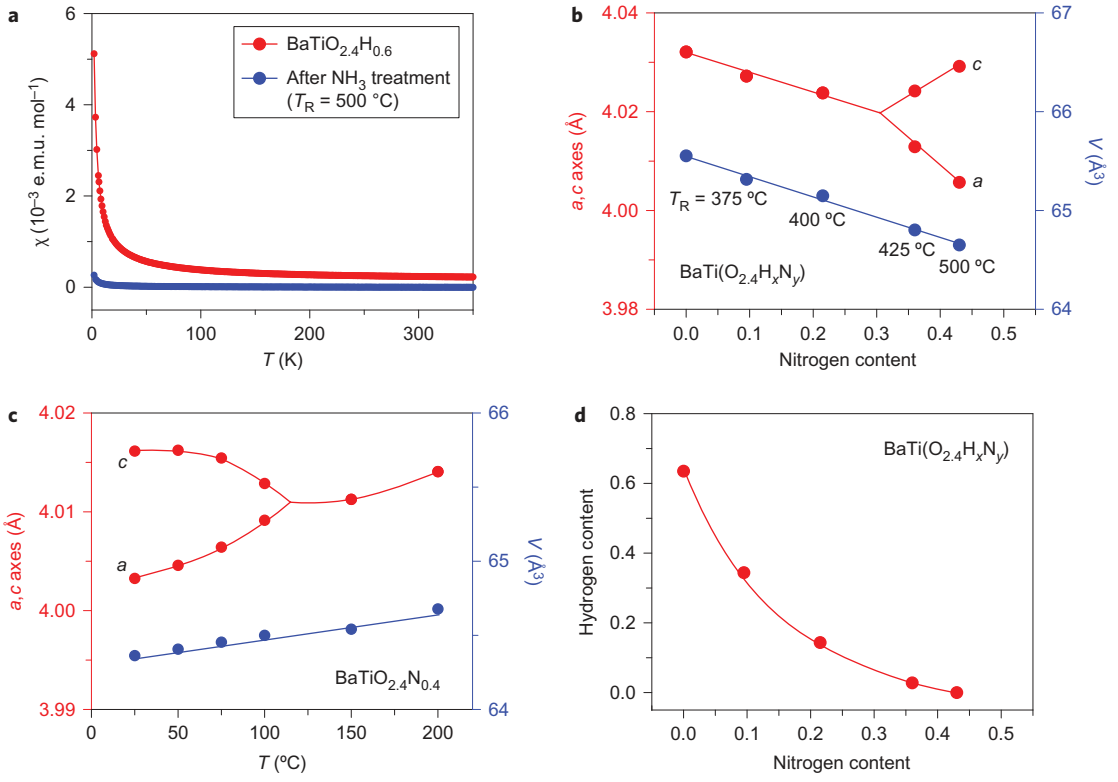

Figure 2 | Anion compositions, cell parameters and magnetism of the NH_3-treated oxyhydrides. a, Temperature dependence of magnetic susceptibilities χ of $BaTiO_{2.4}H_{0.6}$ before (red) and after (blue) the ammonia treatment at $T_R = 500$ °C. The non-magnetic nature of the sample after NH_3 treatment indicates the absence of electrons in the Ti 3*d* t_{2g} band. **b**, Nitrogen content (y) dependence of cell parameters (a, c, V) for $BaTiO_{2.4}H_{0.6}$ and its samples before the reaction ($y = 0$) and ammonolysed at 375 °C, 400 °C, 425 °C and 500 °C. The cell volume decreases with increasing T_R, which implies a gradual oxidation of Ti. A tetragonal distortion is observed for samples with $T_R \geq 425$ °C along the a and c axes, as labelled. **c**, Temperature dependence of the lattice parameters for $BaTiO_{2.4}N_{0.4}$ shows a tetragonal-to-cubic transition at around 100–150 °C, consistent with the SHG results (see Fig. 5a). **d**, The hydrogen content x versus the nitrogen content y, where the x and y values were determined, respectively, by TDS and elemental analysis. The solid lines in **b**–**d** are guides to the eye.

$BaTiO_{2.4}H_{0.6}$ is converted completely into $BaTiO_{2.4}D_{0.6}$ (ref. 16). The present work demonstrates that the hydride thermolability in $BaTiO_{3-x}H_x$ allows H^-/N^{3-} exchange through low-temperature ammonolysis (<500 °C) to yield oxynitride $BaTiO_{3-x}N_{2x/3}$ via oxyhydride–nitride intermediates, as illustrated in Fig. 1. This H^-/N^{3-} exchange is an oxidative reaction that involves a crossover of metal-to-insulator behaviour as well as a cubic-to-tetragonal transition, and the final tetragonal product $BaTi^{4+}O_{3-x}N_{2x/3}$ shows ferroelectric properties at room temperature.

Results and discussion

Sample preparation and characterization. First, a powder sample of $BaTiO_{3-x}H_x$ with $x = 0.60$ ($a = 4.0321(1)$ Å) was synthesized by the CaH_2 reduction of $BaTiO_3$ (100–200 nm), as reported previously[16]. The $BaTiO_{2.40}H_{0.60}$ powder, which contained a tiny amount of TiH_2 impurity (Supplementary Fig. 1 and Supplementary Table 1), was pelletized and heated at various temperatures (reaction temperature T_R, 375–500 °C) for three hours under flowing dry NH_3, and the resulting materials were characterized

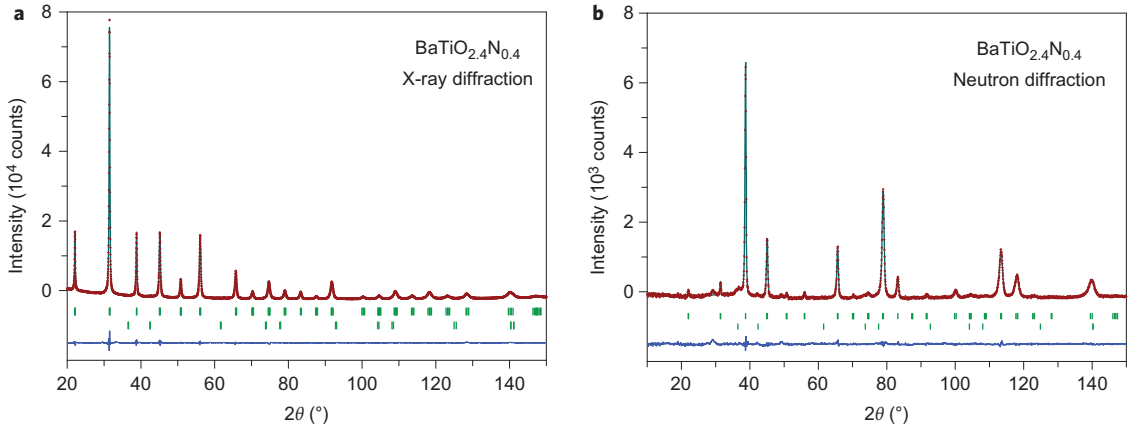

Figure 3 | Structural refinement for $BaTiO_{2.4}N_{0.4}$. a,b, Refined PXRD (**a**) and PND (**b**) patterns of $BaTiO_{2.4}N_{0.4}$ that show the observed (red), calculated (green) and difference (blue) profiles. The upper band and lower band of vertical ticks represent the positions of the calculated Bragg reflections of $BaTiO_{2.4}N_{0.4}$ and TiN (minor impurity), respectively. The PXRD refinement converged successfully to $R_{wp} = 5.12\%$, $R_p = 3.78\%$ and $\chi^2 = 1.20$. The PND refinement also converged to $R_{wp} = 3.86\%$, $R_p = 3.05\%$ and $\chi^2 = 2.71$ (see Supplementary Note 1 for the definition of R_{wp}, R_p and χ^2). The refined parameters are listed in Table 1.

(Fig. 2). Room-temperature laboratory powder X-ray diffraction (PXRD) profiles of samples after the low-temperature ammonolysis (Supplementary Fig. 2) revealed that the cell volume decreased with increasing T_R (Fig. 2b), which implies a gradual increase in the valence of Ti. A continuous colour change from dark blue to green accompanied the reaction. As shown in Fig. 2a, the temperature dependence of the magnetic susceptibility of the sample reacted at $T_R = 500$ °C (sample 1) exhibited a non-magnetic nature throughout the temperature range examined, which indicates an almost complete oxidation to Ti^{4+} (d^0), in stark contrast to the paramagnetic behaviour of the precursor oxyhydride, which consisted of $Ti^{3.4+}$ ($d^{0.6}$) (ref. 16). It is rare that NH_3 acts as an oxidizing agent. This unusual reaction probably arises because only the hydrides, and not the oxides, can leave or be abstracted from the lattice at low temperatures. Such oxidation reactions with NH_3 or other gaseous species can be observed with Ta or Ti in reduced oxidation states, or from other systems in coordination chemistry. For example, Ti metal or TaN react with NH_3 to yield $Ti^{3+}N$ or $Ta_3^{5+}N_5$, and the oxidative addition of H_2 to $Rh^{1+}Cl(PPh_3)_3$ leads to $Rh^{3+}ClH_2(PPh_3)_3$.

We also performed NH_3 reactions (reaction temperature (T_R) = 450–550 °C, three hours) with an oxyhydride of lower hydride content ($BaTiO_{2.62}H_{0.38}$, $a = 4.01141(6)$ Å (see Supplementary Fig. 3 and Supplementary Table 1 for a structural analysis)), which also revealed the lattice expansion as a function of T_R (Supplementary Fig. 4). Measurements with a superconducting quantum interference device showed that almost all of the Ti^{3+} in the precursor was oxidized to Ti^{4+} at $T_R = 550$ °C. The green colour of the product comes from the low-energy photon absorption of intervalence charge transfer and implies a tiny amount of Ti^{3+}.

Several chemical analyses were conducted to determine the anion composition in the terminal non-magnetic compounds (samples 1 and 2). Quadrupole mass spectroscopy (QMS) for samples 1 and 2 showed the absence of hydrogen. Elemental analysis (combustion analysis) revealed the presence of a considerable amount of nitrogen, 2.8 wt% (sample 1) and 1.3 wt% (sample 2). Furthermore, *in situ* QMS during the NH_3 reaction exhibited no trace of H_2O. This means that the oxygen content remained the same because O^{2-} is more strongly bound to the metal centre than H^-. Thus, nitride anions should replace only the labile hydride ions. The elemental analysis gave compositions of $BaTiO_{2.40}N_{0.43}$ (sample 1) and $BaTiO_{2.62}N_{0.21}$ (sample 2), with corresponding Ti valences of +4.09 and +3.87, both of which are in fairly good accordance with the non-magnetic nature.

We also found a tetragonal distortion of the unit cell in the samples ($x = 0.60$) ammonolysed at $T_R \geq 425$ °C (Fig. 2b). As described later, the tetragonal distortion is associated with the absence of conduction electrons in a Ti $3d$ t_{2g} band. The room-temperature lattice constants of sample 1 (ammonolysed at 500 °C) were estimated to be $a = 4.0057(7)$ Å and $c = 4.0292(7)$ Å ($c/a = 1.0059(3)$). Similarly, the $x = 0.38$ samples reacted at 500 °C and 550 °C exhibited a tetragonal distortion (Supplementary Fig. 4). An *in situ* synchrotron PXRD study on sample 1 revealed a tetragonal-to-cubic transition at around 100–150 °C (Fig. 2c), which was accompanied by a paraelectric-to-ferroelectric phase transition, as is discussed later in the section Ferroelectricity in $BaTiO_{2.4}N_{0.4}$.

Despite the low-temperature reaction, no appreciable peak broadening was seen in the PXRD and powder neutron diffraction (PND) profiles for sample 1. This indicates a compositional uniformity and we performed a Rietveld structural refinement as another verification of the anionic composition. Given the tetragonal symmetry ($c/a > 1$) and the similarity in T_C with the ferroelectric $BaTiO_3$ (150 °C), it is natural to build a structural model on the basis of $BaTiO_3$ ($P4mm$ space group), in which Ba atoms are placed at the 1*a* site, Ti atoms at the 1*b* site and O/N atoms at the 1*b* and 2*c* sites with a random distribution of the anions. An oxygen-deficient $BaTiO_{3-\delta}$ was assumed for the PXRD refinement because of the negligible X-ray scattering contrast between O and N, and the composition of $BaTiO_{2.40}N_y$ was assumed for the PND refinement. The ammonolysis causes the small TiH_2 impurity in the oxyhydride precursor to convert into TiN, which was included in both refinements as a secondary phase.

As shown in Fig. 3a and Table 1, the XRD refinement converged successfully, with the anion-vacancy content refined to $\delta = 0.14(1)$ (meaning $BaTiO_{2.40}N_{0.46(1)}$). The PND refinement also converged (Fig. 3b), and the nitrogen content y was refined to 0.39(7) ($BaTiO_{2.40}N_{0.39(7)}$). Given that the terminal oxynitrides are non-magnetic, the composition of sample 1 should be $BaTiO_{2.40}N_{0.40}$. The PXRD and PND refinements for sample 2 using the $BaTiO_3$-type structure (Supplementary Fig. 5 and Supplementary Table 1), respectively, gave $BaTiO_{2.87(3)}$ (meaning $BaTi^{3.99+}O_{2.62}N_{0.25(3)}$) and $BaTi^{3.96+}O_{2.62}N_{0.24(1)}$ with the Ti valence very close to +4. Therefore, we conclude in general that the hydride lability in $BaTiO_{3-x}H_x$ allows low-temperature oxidative nitridization to give the non-magnetic tetragonal phase of $BaTi^{4+}O_{3-x}N_{2x/3}$.

We compared the present result to those of previous works on nitrogen-doped $BaTiO_3$. $BaTiO_{2.85-y}N_{0.1}$ was obtained by calcination of $BaCO_3$ and TiO_2 at 950 °C under an NH_3 flow[17].

Table 1 | Refined PND (PXRD) structural parameters of $BaTiO_{2.4}N_{0.4}$.

Atom	Site	*x*	*y*	*Z*	Occupancy	$100U_{iso}$ (Å^2)
Ba	1*a*	0	0	0	1	0.4(2) (0.74(1))
Ti	1*b*	0.5	0.5	0.48(1) (0.487(3))	1	0.7(2) (0.91(7))
O1	1*b*	0.5	0.5	0.004(10) (−0.018(4))	0.8 (0.954(5))	0.9(6) (0.5(1))
N1	1*b*	0.5	0.5	0.004(10)	0.13(4)	0.9(6)
O2	2*c*	0.5	0	0.500(9) (0.523(6))	0.8 (0.954(5))	0.9(3) (0.5(1))
N2	2*c*	0.5	0	0.500(9)	0.13(3)	0.9(3)

Space group *P4mm*, a = 4.0087(2) Å (4.00883(6) Å), c = 4.0223(4) Å (4.02058(10) Å), R_{wp} = 5.12% (3.86%), R_p = 3.78% (3.05%), χ^2 = 1.20 (2.71). Supplementary Note 1 gives the definitions of R_{wp}, R_p and χ^2. U_{iso}, isotropic temperature factor. The PND and PXRD patterns are shown in Fig. 3.

However, it exists as a two-phase mixture and its nitrogen amount is much smaller. $(Ba_xSr_{1-x})_{1+y}Ti_{1-y}O_{3-z}N_z$ thin films synthesized by a molecular beam epitaxy technique have a negligible amount of nitrogen (N/O ratio < 0.001)[18]. As shown below, in addition to this significant quantitative difference, our labile hydride strategy enables a versatile control of the nitrogen content by the ammonolysis temperature (and possibly reaction time) and by precursors with different hydride concentrations.

Metal-to-insulator crossover via mixed O–H–N intermediates. Oxyhydride–nitrides $BaTiO_{3-x}H_zN_y$ (where $x > y + z$) can also be formed at lower reaction temperatures with NH_3. The amount of hydride/nitride was examined by elemental analysis and thermal desorption spectroscopy (TDS). The $x = 0.6$ sample at T_R = 400 °C was determined to be $BaTi^{3.6+}O_{2.4}H_{0.14}N_{0.22}$. Figure 2d illustrates a correlation between the hydride and nitride concentration. As T_R is increased, the N content (y) increases and the H content (z) decreases. The PXRD profiles of the intermediate oxyhydride–nitride samples (including $BaTiO_{2.4}H_{0.34}N_{0.10}$ obtained at T_R = 375 °C) consist of relatively sharp peaks (Supplementary Fig. 2), which suggests a uniform anion composition. Apparently, trivalent N^{3-} ions are mobile even at low temperatures during the NH_3 reaction. Although there are very few vacancies in $BaTiO_{3-x}H_x$ (ref. 16), the vacancy amount ($x - y - z$ in $BaTiO_{3-x}H_zN_y$) must increase on ammonolysis, given that the final composition of $BaTiO_{3-x}N_{2x/3}$ has a vacancy amount of $x/3$ (10% in $BaTiO_{2.4}N_{0.4}$). We speculate that the reduced H^- amount, which is unfavourable for anion diffusion, is compensated by the increased vacancy amount, which is favourable for anion diffusion, and thereby helps the reaction to reach the terminal oxynitride.

A few oxynitrides, such as layered $Li_{0.88}Nb_3(O_{0.13}N_{0.87})$ and anatase TaON, are known to exhibit electric conductivity or superconductivity[19,20], but the precise and extensive tuning of carrier concentration is rather difficult, which notably limits the extensive investigation of physical properties of oxynitrides. From the metallic and insulating behaviour in $SrTiO_{3-x}H_x$ ($x \approx 0.3$)[21] and $BaTiO_{3-x}N_{2x/3}$, respectively, one can expect controlled transport properties by continuous oxidative nitridization of the oxyhydride to the oxynitride via oxyhydride–nitrides. To demonstrate this, epitaxial thin films of $SrTiO_{2.75}H_{0.25}$ on a (La,Sr)(Al,Ta)O_3 (LSAT) substrate were grown as described in Yajima *et al.*[21] and reacted with NH_3 at various temperatures up to 550 °C. The presence of nitrogen and the absence of hydrogen for the terminal film (with T_R = 550 °C) was checked, respectively, by X-ray photoemission spectroscopy (XPS) (Supplementary Fig. 6) and TDS. With increasing T_R, the electrical resistivity showed an increase by four orders of magnitude, accompanied by a drastic reduction in carrier density (Fig. 4). A semiconducting or insulating temperature dependence was seen for the films treated above 450 °C.

Ferroelectricity in $BaTiO_{2.4}N_{0.4}$. Recently, it was highlighted that $ATaO_2N$ (A = Ba, Sr) is tetragonal and has an unusual anion order that originates from a *cis* coordination within the TaO_4N_2 octahedron[6,22]. However, this tetragonal phase is stable at much higher temperatures (up to 700 °C) and its tetragonality is not significant. The dependence of c/a on the nitrogen content (1.0069 in $BaTiO_3$ (140 nm)[23], 1.0039 in $BaTiO_{2.62}N_{0.24}$ and 1.0034 in $BaTiO_{2.4}N_{0.4}$) shows that the solid-solution $BaTiO_{3-x}N_{2x/3}$ probably belongs to the same ferroelectric phase. Optical second-harmonic generation (SHG) and piezoresponse force microscopy (PFM) are powerful tools for probing non-centrosymmetry and ferroelectricity in materials. Figure 5a shows the temperature dependence of SHG intensity for a $BaTiO_{2.4}N_{0.4}$ bulk sample, measured in reflection geometry with an 800 nm fundamental beam (Ti:sapphire laser, 80 fs pulses, 1 kHz repetition rate). A finite SHG signal is clearly observed at room temperature, which indicates that the tetragonal $BaTiO_{2.4}N_{0.4}$ has a non-centrosymmetric structure. On heating, the SHG intensity steeply decreases and diminishes at about 150 °C, at which the

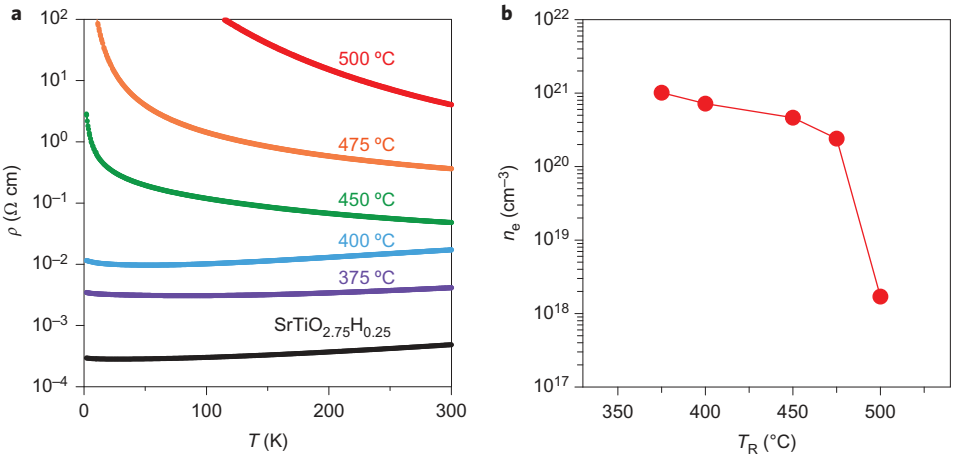

Figure 4 | Systematic evolution of transport properties from oxyhydride $SrTiO_{2.75}H_{0.25}$ to oxyhydride–nitride $SrTiO_{2.75}H_zN_y$ ($y + z < 0.25$) to oxynitride $SrTiO_{2.75}N_y$ ($y \approx 0.16$). **a**, Temperature dependence of resistivity. From bottom to top, the $SrTiO_{2.75}H_{0.25}$ film and its ammonia-treated films at T_R = 375, 400, 450, 475 and 500 °C. With increasing T_R, the electrical resistivity increases and a metal-to-insulator crossover can be seen. **b**, The carrier density n_e of the films estimated from Hall measurements as a function of T_R demonstrates a systematic reduction of n_e with T_R.

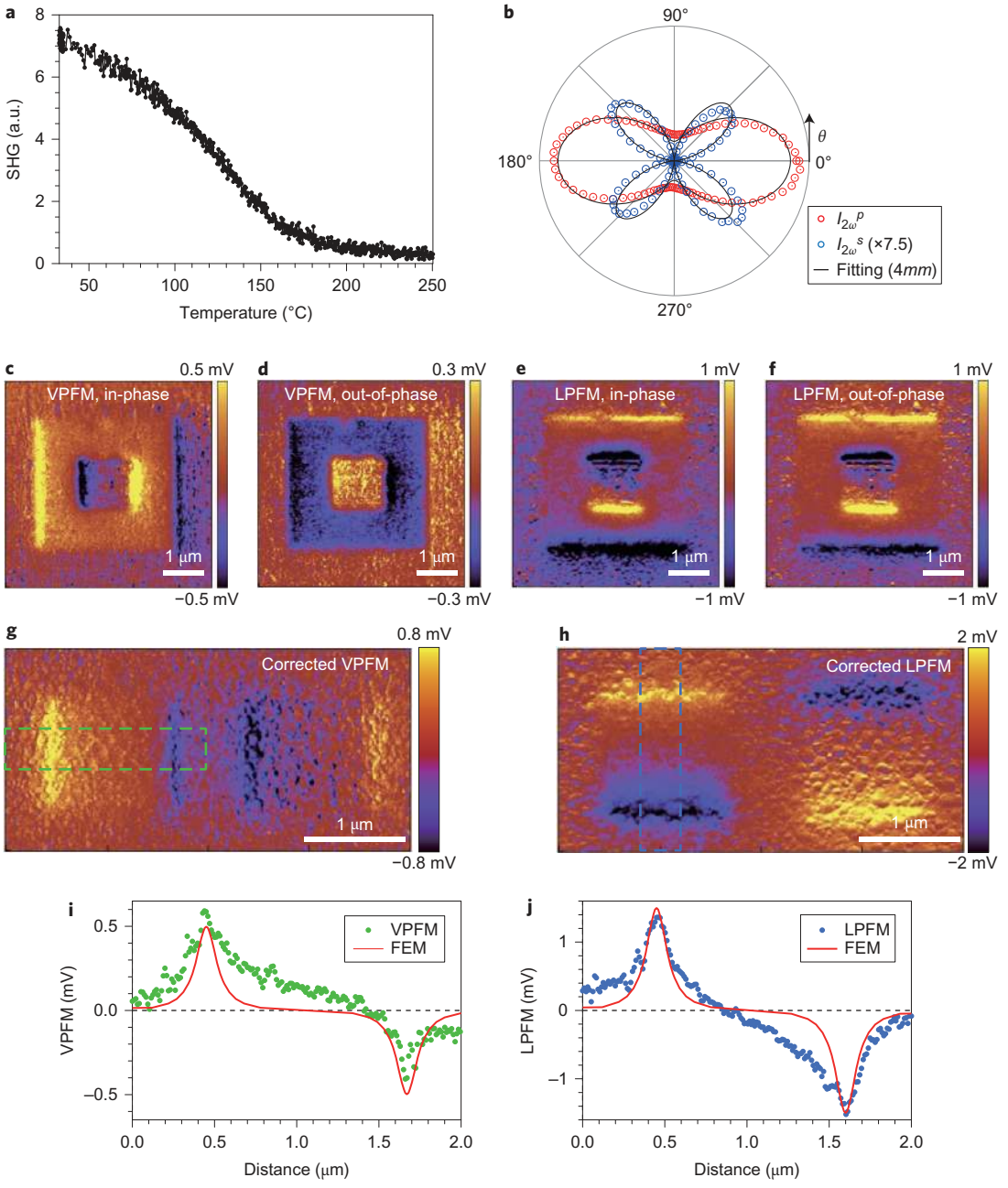

Figure 5 | Ferroelectric properties of $BaTiO_{2.4}N_{0.4}$. **a**, The temperature dependence of SHG intensity for the $BaTiO_{2.4}N_{0.4}$ bulk sample reveals a centrosymmetric-to-non-centrosymmetric phase transition around 150 °C. **b**, Variation of *p*- and *s*-polarized SHG intensities, $I_{2\omega}{}^{p}$ and $I_{2\omega}{}^{s}$, for the $BaTiO_{2.4}N_{0.4}$ thin film as a function of rotation angle of the electric field of the fundamental light, θ, measured in the transmission set-up (Supplementary Fig. 8). The polar plots fitted well using a *4mm* model with a four-fold axis perpendicular to the film. **c**–**f**, In-phase VPFM (**c**), out-of-phase VPFM (**d**), in-phase LPFM (**e**) and out-of-phase LPFM (**f**) images taken after the electric-field poling (Supplementary Fig. 9), which clearly demonstrate polarization switching. **g**,**h**, Corrected VPFM (**g**) and LPFM (**h**) images obtained by poling in a different way (Supplementary Fig. 10). **i**,**j**, Averaged line profiles of the dashed rectangle areas in **g** and **h**, respectively. Also shown is the in-plane piezoelectric displacement simulated by FEM. Here the in-plane displacement is the piezoelectric displacement in the scanning direction when a tip is scanned across 180° up and down domain walls (Supplementary Fig. 11). The VPFM response is contributed not by out-of-plane piezoelectric displacements, but by a buckling effect of the PFM tip. a.u., arbitrary units.

temperature dependence of the lattice parameters shows the tetragonal-to-cubic transition (Fig. 2c). This transition temperature is close to that of $BaTiO_3$.

To confirm the point-group symmetry of tetragonal $BaTiO_{2.4}N_{0.4}$, we performed SHG polarimetry at room temperature using a thin film. The presence and composition of nitrogen in the $BaTiO_{2.4}N_{0.4}$ film was checked with XPS (Supplementary Fig. 7) and TDS. Figure 5b shows the dependence of SHG intensity on the direction of polarization of the fundamental light for the $BaTiO_{2.4}N_{0.4}$ thin film collected in the transmission geometry (Supplementary Fig. 8). The polar plots for both *p* and *s* polarizations, $I_{2\omega}{}^{p}$ and $I_{2\omega}{}^{s}$, respectively, are reproduced well by curves derived by *4mm* symmetry with a four-fold axis perpendicular to the film, in good agreement with the PXRD results.

Figure 5c–f presents vertical (V) and lateral (L) in-phase and out-of-phase PFM scanning images for the $BaTiO_{2.4}N_{0.4}$ film, taken after being electrically poled (Supplementary Fig. 9). One can clearly see PFM signal contrasts in the region where the poling

was done, which demonstrates the ferroelectric nature. We also performed a PFM imaging after poling in a different way. The corrected VPFM and LPFM images are shown in Fig. 5g,h. To understand the PFM patterns, piezoelectric displacements were calculated using finite-element methods (FEMs). Figure 5i,j show line profiles of the VPFM and LPFM signals averaged within the dotted rectangles in Fig. 5g,h, respectively, along with the calculated piezoelectric displacements. Both the VPFM and LPFM line profiles are very similar to a simulated curve for the in-plane displacement. The VPFM response exhibits a similar behaviour to the in-plane displacement rather than to the out-of-plane displacement (Supplementary Fig. 10). This is because the PFM tip used in the present experiments is sensitive to buckling, which is detected as a VPFM response[24]. Thus, the PFM responses of the $BaTiO_{2.4}N_{0.4}$ film, together with the SHG observation, corroborate its ferroelectricity.

Perspectives. A growing number of transition-metal oxyhydrides have been discovered since 2002, and especially within the past few years, namely $ATiO_{3-x}H_x$ (A = Ca, Sr, Ba)[25], $LaSrCoO_3H_{0.7}$ (ref. 26), $SrVO_2H$ (ref. 27), $Sr_{n+1}V_nO_{2n+1}H_n$ ($n = 1$, 2)[27,28], $SrCrO_2H$ (ref. 29) and $LaFeAsO_{1-x}H_x$ (ref. 30). However, most studies have focused on their syntheses and physical properties. What we show here is that the lability of the hydride makes an oxyhydride useful for a preparatory reaction. We believe that this reactivity applies to oxyhydride systems more generally, and that it should be possible to prepare, through this topochemical route, a large number of new transition-metal oxynitrides with interesting transport and magnetic properties. Such studies are in progress in our laboratory and will be reported elsewhere in due course. For example, although $BaTiO_{3-x}N_{2x/3}$ has a random distribution of nitride in the structure, anion-ordered oxynitride might result if an anion-ordered oxyhydride is used as a precursor. Furthermore, this labile hydride strategy is not limited to the synthesis of oxynitrides, but also applies to the synthesis of other mixed anionic compounds through anion-exchange reactions, such as H^-/F^-, H^-/OH^- or H^-/S^{2-}, at low temperatures.

Methods

Precursor oxyhydrides $BaTiO_{3-x}H_x$ ($x = 0.60$, 0.38) were synthesized by a topochemical reaction of $BaTiO_3$ with a particle size of 100–200 nm (Sakai Chemical Industry) using a 3 mol excess of CaH_2 (99%, Aldrich) in a sealed, evacuated Pyrex tube at 580 °C for four days ($x = 0.38$) and seven days ($x = 0.60$)[16]. Before the hydride reduction, $BaTiO_3$ was preheated at 150 °C overnight under vacuum to remove completely any adsorbed water, a crucial process to achieve the target hydride compositions in a reproducible manner. The oxyhydrides prepared were washed with 0.1 M NH_4Cl/methanol to remove excess CaH_2 and CaO and were dried at 100 °C under vacuum. Pelletized $BaTiO_{3-x}H_x$ (0.5 g) was placed in a tubular furnace. The furnace was purged with dry nitrogen and then with dry NH_3 before heating to remove any oxygen and moisture. Under a dry NH_3 flow (300 ml min^{-1}), the sample was heated to the target temperature (T_R = 375–550 °C) at a heating rate of 100 °C per hour, held for three hours and cooled to room temperature.

PXRD patterns were recorded at room temperature with a Bruker D8 ADVANCE diffractometer with Cu $K\alpha$ radiation. High-resolution synchrotron PXRD experiments for the structural refinement were performed using a large Debye–Scherrer camera installed at SPring-8 BL02B2 of the Japan Synchrotron Radiation Research Institute (JASRI), with $\lambda = 0.7774225$ Å and 0.399261 Å for room-temperature and high-temperature (up to 200 °C) measurements, respectively. The sieved (32 μm) fine powder sample was loaded into a capillary (0.2 mm internal diameter (i.d.) for room-temperature and 0.1 mm i.d. for high-temperature experiments). The capillary was rotated during the measurements for a better averaging of the powder-pattern data. PND experiments were carried out at room temperature with approximately 3 g of samples to BT1 specifications ($\lambda = 1.5406$ Å, Cu (311) monochromator) at the National Institute of Standards and Technology. The diffraction data were analysed by the Rietveld method using the RIETAN-FP program[31]. TDS (ESCO, Ltd) was used to determine the hydrogen amount in the specimen. The nitride content of the specimen was determined by combustion analysis (Yanaco CHN Corder).

Epitaxial $ATiO_3$ films (A = Sr, Ba) were grown on a LSAT substrate by pulsed laser deposition with a KrF excimer laser (λ, 248 nm; energy density, 0.7 J cm^{-2}; pulse frequency, 1 Hz). We also fabricated a $BaTiO_3$ film on LSAT with a $SrRuO_3$ conducting buffer layer for the PFM measurements. The substrate temperature was kept at 700 °C, and the oxygen partial pressure was 5.0×10^{-2} Pa. The oxide films were reduced to $ATiO_{3-x}H_x$ using CaH_2 at 530 °C for one day, as reported[21]. The nitridization reaction of the $ATiO_{3-x}H_x$ films with NH_3 gas was conducted in a sealed, evacuated Pyrex tube in a temperature range of 375–500 °C for three hours. As the NH_3 gas source, a 1:1 mixture of $NaNH_2$ and NH_4Cl (40 mg) was used, which was placed separately from the film. Out-of-plane XRD and reciprocal space mapping of the oxynitride film were measured to check the epitaxy, and XPS and TDS were conducted to probe and quantify the nitrogen (Supplementary Figs 6 and 7). In XPS measurements, the N 1*s* peaks were observed around 396 eV, which suggests Ti–N bonding[1,18]. The nitrogen amount was determined as 2.9 wt% from TDS, which is very close to that in the bulk $BaTiO_{2.4}N_{0.4}$ sample (2.8 wt%). The temperature dependence of electric resistivity was measured by a standard four-probe method along the in-plane direction where Au(30 nm)/Ti(5 nm) electrodes were deposited by electron-beam evaporation. The carrier density of the films was estimated from Hall measurements.

Optical SHG was measured for $BaTiO_{2.4}N_{0.4}$ bulk and thin-film samples using an 800 nm fundamental beam (Ti:sapphire laser, 80 fs pulses, 1 kHz repetition rate). The SHG signals from the bulk sample were collected in reflection geometry between 30 and 250 °C. The SHG polarimetry measurements were performed at room temperature for the thin film on an LSAT substrate in transmission geometry. Supplementary Fig. 8 illustrates the experimental geometry in the transmission geometry.

PFM measurements were performed for the $BaTiO_{2.4}N_{0.4}$ thin film on an LSAT substrate with a $SrRuO_3$ conducting buffer layer by using an atomic force microscope (AFM) system (Bruker, Dimension Icon). A chromium/gold-coated conducting AFM tip (HQ:NSC19/Cr-Au, MikroMasch) was utilized. The experimental geometry and poling process are shown in Supplementary Fig. 9. A background correction was done according to the methods described in Jungk *et al.*[32] and Lei *et al.*[33] (Supplementary Fig. 12). An FEM simulation was conducted to calculate the piezoelectric displacements by using the commercial software ANSYS. A domain-structure model used in this study is illustrated in Supplementary Fig. 10. More details about the FEM simulations are described in Lei *et al.*[24].

Received 12 June 2015; accepted 8 September 2015; published online 19 October 2015

References

1. Asahi, R., Morikawa, T., Ohwaki, T., Aoki, K. & Taga, Y. Visible-light photocatalysis in nitrogen-doped titanium oxides. *Science* **293,** 269–271 (2001).
2. Maeda, K. *et al.* Photocatalyst releasing hydrogen from water. *Nature* **440,** 295 (2006).
3. Jansen, M. & Letschert, H. P. Inorganic yellow–red pigments without toxic metals. *Nature* **404,** 980–982 (2000).
4. Kim, Y. I., Woodward, P. M., Baba-Kishi, K. Z. & Tai, C. W. Characterization of the structural, optical, and dielectric properties of oxynitride perovskites AMO_2N (A = Ba, Sr, Ca; M = Ta, Nb). *Chem. Mater.* **16,** 1267–1276 (2004).
5. Kim, Y. I. *et al.* Epitaxial thin-film deposition and dielectric properties of the perovskite oxynitride $BaTaO_2N$. *Chem. Mater.* **19,** 618–623 (2007).
6. Page, K. *et al.* Local atomic ordering in $BaTaO_2N$ studied by neutron pair distribution function analysis and density functional theory. *Chem. Mater.* **19,** 4037–4042 (2007).
7. Oka, D. *et al.* Possible ferroelectricity in perovskite oxynitride $SrTaO_2N$ epitaxial thin films. *Sci. Rep.* **4,** 4987 (2014).
8. Jorge, A. B. *et al.* Large coupled magnetoresponses in $EuNbO_2N$. *J. Am. Chem. Soc.* **130,** 12572–12573 (2008).
9. Ebbinghaus, S. G. *et al.* Perovskite-related oxynitrides—recent developments in synthesis, characterisation and investigations of physical properties. *Prog. Solid State Chem.* **37,** 173–205 (2009).
10. Fuertes, A. Chemistry and applications of oxynitride perovskites. *J. Mater. Chem.* **22,** 3293–3299 (2012).
11. Gomathi, A., Reshma, S. & Rao, C. N. R. A simple urea-based route to ternary metal oxynitride nanoparticles. *J. Solid. State Chem.* **182,** 72–76 (2009).
12. Watanabe, T., Tajima, K., Li, J. W., Matsushita, N. & Yoshimura, M. Low-temperature ammonothermal synthesis of $LaTaON_2$. *Chem. Lett.* **40,** 1101–1102 (2011).
13. Clarke, S. J., Guinot, B. P., Michie, C. W., Calmont, M. J. C. & Rosseinsky, M. J. Oxynitride perovskites: synthesis and structure of $LaZrO_2N$, $NdTiO_2N$, and $LaTiO_2N$ and comparison with oxide perovskites. *Chem. Mater.* **14,** 288–294 (2002).
14. Tessier, F. & Marchand, R. Ternary and higher order rare-earth nitride materials: synthesis and characterization of ionic–covalent oxynitride powders. *J. Solid State Chem.* **171,** 143–151 (2003).
15. McAuley, A. & Hague, D. N. *Inorganic Reaction Mechanisms* (RSC Publishing, 1977).
16. Kobayashi, Y. *et al.* An oxyhydride of $BaTiO_3$ exhibiting hydride exchange and electronic conductivity. *Nature Mater.* **11,** 507–511 (2012).
17. Bräuniger, T., Müller, T., Pampel, A. & Abicht, H. Study of oxygen–nitrogen replacement in $BaTiO_3$ by ^{14}N solid-state nuclear magnetic resonance. *Chem. Mater.* **17,** 4114–4117 (2005).

18. David, A. *et al.* High-throughput synthesis and characterization of $(Ba_xSr_{1-x})_{1+y}Ti_{1-y}O_{3-\delta}$ and $(Ba_xSr_{1-x})_{1+y}Ti_{1-y}O_{3-z}N_z$ perovskite thin films. *Cryst. Growth Des.* **14,** 523–532 (2014).
19. Motohashi, T., Ito, M., Masubuchi, Y., Wakeshima, M. & Kikkawa, S. Crystal structure and superconducting properties of hexagonal lithium–niobium oxynitride. *Inorg. Chem.* **51,** 11184–11189 (2012).
20. Suzuki, A. *et al.* High-mobility electron conduction in oxynitride: anatase TaON. *Chem. Mater.* **26,** 976–981 (2013).
21. Yajima, T. *et al.* Epitaxial thin films of $ATiO_{3-x}H_x$ (A= Ba, Sr, Ca) with metallic conductivity. *J. Am. Chem. Soc.* **134,** 8782–8785 (2012).
22. Yang, M. *et al.* Anion order in perovskite oxynitrides. *Nature Chem.* **3,** 47–52 (2011).
23. Yashima, M. *et al.* Size effect on the crystal structure of barium titanate nanoparticles. *J. Appl. Phys.* **98,** 014313 (2005).
24. Lei, S. *et al.* Reply to "Comment on 'Origin of piezoelectric response under a biased scanning probe microscopy tip across a 180° ferroelectric domain wall'". *Phys. Rev. B* **89,** 226102 (2014).
25. Sakaguchi, T. *et al.* Oxyhydrides of (Ca,Sr,Ba)TiO_3 perovskite solid solutions. *Inorg. Chem.* **51,** 11371–11376 (2012).
26. Hayward, M. A. *et al.* The hydride anion in an extended transition metal oxide array: $LaSrCoO_3H_{0.7}$. *Science* **295,** 1882–1884 (2002).
27. Romero, F. D. *et al.* Strontium vanadium oxide–hydrides: 'square-planar' two-electron phases. *Angew. Chem. Int. Ed.* **53,** 7556–7559 (2014).
28. Bang, J. *et al.* Hydrogen ordering and new polymorph of layered perovskite oxyhydrides: $Sr_2VO_{4-x}H_x$. *J. Am. Chem. Soc.* **136,** 7221–7224 (2014).
29. Tassel, C. *et al.* Direct synthesis of chromium perovskite oxyhydride with a high magnetic transition temperature. *Angew. Chem. Int. Ed.* **126,** 10545–10548 (2014).
30. Iimura, S. *et al.* Two-dome structure in electron-doped iron arsenide superconductors. *Nature Commun.* **3,** 943 (2012).
31. Izumi, F. & Momma, K. Three-dimensional visualization in powder diffraction. *Solid State Phenom.* **130,** 15–20 (2007).
32. Jungk, T., Hoffmann, A. & Soergel, E. Quantitative analysis of ferroelectric domain imaging with piezoresponse force microscopy. *Appl. Phys. Lett.* **89,** 163507 (2006).
33. Lei, S. *et al.* Origin of piezoelectric response under a biased scanning probe microscopy tip across a 180° ferroelectric domain wall. *Phys. Rev. B* **86,** 134115 (2012).

Acknowledgements

This work is supported by FIRST and CREST programmes of the Japan Science and Technology Agency. H.A., S.L. and V.G. acknowledge support from the National Science Foundation grant numbers DMR-1420620 and DMR-1210588. H.A. acknowledges support from Japan Society for the Promotion of Science for Research Abroad (No. 25-185). The synchrotron radiation experiments were performed at the BL02B2 of SPring-8 with the approval of the JASRI.

Author contributions

T. Yajima and F.T. contributed equally. T. Yajima, F.T. and H.K. conceived and designed the study. F.T., K.A., M.O., W.Y. and T. Yajima performed the synthesis, laboratory PXRD, synchrotron PXRD, XPS and elemental analysis. T.Yam., C.M.B., M.A.G. and H.K. obtained the neutron data. The structural refinement was performed by K.A., T. Yamamoto and T. Yajima. W.Y. and T. Yajima fabricated the thin films. H.A., K.F., S.L., V.G. and K.T. conducted the SHG and PFM measurements and FEM simulations. All authors discussed the results. F.T. and H.K. wrote the manuscript, with contributions and feedback from all the authors, mainly T. Yajima, Y.K., H.A. and K.F.

Additional information

Supplementary information is available in the online version of the paper. Reprints and permissions information is available online at www.nature.com/reprints. Correspondence and requests for materials should be addressed to H.K.

Competing financial interests

The authors declare no competing financial interests.